Polymer Chemistry

Accepted Manuscript

ROYAL SOCIETY OF CHEMISTRY

www.rsc.org/polymers

Cite this: DOI: 10.1039/c0xx00000x

www.rsc.org/xxxxxx

ARTICLE TYPE

Highly Stable Hybrid Selenophene-3,4-Ethylenedioxythiophene as Electrically Conducting and Electrochromic Polymers

Baoyang Lu[a,b], Shijie Zhen[b], Shimin Zhang[b], Jingkun Xu[a,b,*], Guoqun Zhao[a,*]

Received (in XXX, XXX) Xth XXXXXXXXX 200X, Accepted Xth XXXXXXXXX 200X

DOI: 10.1039/b000000x

A family of four novel selenophene-EDOT oligomers were synthesized using Stille coupling and electropolymerized to form highly stable conducting hybrid polymers with excellent electrochromic properties. Structure-property relationships of the oligomers and hybrid polymers, including electrochemical, electronic and optical properties, quantum chemistry calculations and morphology, were systematically explored. The oligomer precursors with planar structures exhibit blue to orange emission characteristics with quantum yields ranging from 1.5 to 9.0%, which may be used as building blocks for the rational design of fluorescent conjugated systems with enhanced main chain planarity. Cyclic voltammetry shows low oxidation potentials ranging from 0.53 to 0.89 V *vs.* Ag/AgCl, leading to the facile electrodeposition of uniform hybrid polymer films with outstanding electroactivity and stability at low oxidation potentials. The obtained hybrid polymers featured the advantageous combination of polyselenophene and PEDOT, such as lower band gap and better planarity of polyselenophene, high conductivity, transparency and excellent stability of PEDOT. The hybrid polymers show planar π-conjugated backbones with band gaps ranging from 1.54 to 1.75 eV and electrochromic nature with color changing from purplish, reddish and saturated blue in the reduced form to transmissive sky blue/green upon oxidation. Further kinetic studies demonstrated the hybrid polymers revealed decent contrast ratios (22~36%), favorable coloration efficiencies (~200 cm^2 C^{-1}), low switching voltages, fast response time (0.5 s), excellent stability and color persistence. These materials provide more plentiful electrochromic colors and hold promise for display applications.

1. Introduction

Conjugated oligomers/polymers have received huge attention because of recent progress in solar cells, OLEDs, organic electrochromics, and organic field effect transistors, etc. Stability, conductivity, rigidity/planarity, and band gap in the semiconductor region are among the main requirements for organic electronic materials toward specific applications. In the conducting polymer family, in sharp contrast to oligo- and polythiophenes extensively employed in organic electronics, the research field of oligo-/polyselenophenes has just been established most recently.[1,2] Compared with other types of conducting polymers, oligo-/polyselenophenes exhibit several special properties and advantages, such as lower band gap, more planar backbone, stronger intermolecular interactions (including Se-Se interactions), greater degree of doping, etc.,[1,2] which makes them excellent candidates for applications in organic electronic materials, such as electrochromics and photovoltaic cells.[3-10] Great strides in polyselenophenes have been achieved over the last several years. Besides parent polyselenophene,[11-16] several typical polyselenophenes with excellent performances have been recently reported for optoelectronic applications (their structures are shown in Scheme 1), such as poly(3,4-ethylenedioxyselenophene),[3] poly(3,4-ethylenedithioselenophene),[4] poly(*n*-hexyl-3,4-ethylenedioxyselenophene),[5] poly(alkyl-3,4-ethylenedioxyselenophenes),[6] thieno-/selenolo-fused polyselenophene,[7] polyselenopheno[3,4-*b*]selenophene,[8] poly(3,4-propylenedioxyselenophene),[17] poly(3-alkylselenophene),[18] etc., and several selenophenes-based hybrid polymers,[7,8,19-24] leading to the availability of promising polyselenophene materials. Most recently, our group investigated the thermoelectric performances of different types of polyselenophene and found that polyselenophene exhibits very high Seebeck coefficient (>180 V K^{-1}) and holds promise for thermoelectrics.[25] However, despite these efforts devoted to this research field, the fundamental research and applications of polyselenophenes are far from prosperity and still have significant

[a] *Key Laboratory for Liquid-Solid Structural Evolution and Processing of Materials (Ministry of Education), Shandong University, Ji'nan, Shandong 250061, PR China*

[b] *School of Pharmacy, Jiangxi Science & Technology Normal University, Nanchang 330013, China*

Tel: +86-791-88537967, Fax: +86-791-83823320; (J. Xu)

Tel: +86-531-88393238; Fax: +86-531-88392811 (G. Zhao).

Email: xujingkun@tsinghua.org.cn and zhaogq@sdu.edu.cn.

†Electronic Supplementary Information (ESI) available. See DOI: 10.1039/b0000.

scope for development. The design and synthesis of novel polyselenophenes-based polymers with improved properties suffice for applications are still very necessary and significant, and apparently also a considerable challenge.

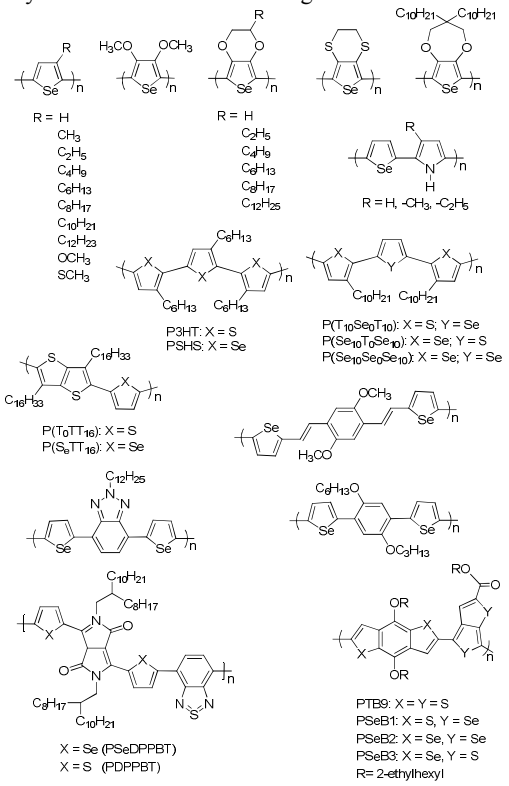

Scheme 1 Recently reported structures of polyselenophenes and their based conjugated systems for optoelectronic applications.

For parent polyselenophene, the electrical conductivity prepared either by chemical polymerization or by electrochemical polymerization was quite low (around the orders of 10^{-4}~10^{-2} S cm^{-1}).[1] Even though it could be improved to 10^{-1} S cm^{-1} by electropolymerization in novel electrolytes Lewis acid boron trifluoride diethyl etherate or ionic liquid $bmimPF_6$ in recent reports,[11,12] the values are still much lower than that of polythiophene (10^{1}~10^{2} S cm^{-1}).[1] Until recently, low conductivity, the lack of a well-defined electrochemical response by polyselenophenes, plus the lack of suitable synthetic methods to prepare substituted selenophene-based monomeric precursors hampered the development of polyselenophene-type polymers. Indeed, the low conductivity and poor electrochemical behavior of polyselenophenes may result from their instability during oxidative polymerization of the monomers and the lack of suitable selenophene precursors for polymerization.

Poly(3,4-ethylenedioxythiophene), or PEDOT, is probably the best conducting polymer available in terms of conductivity, processability (PEDOT:PSS), and stability.[26] Furthermore, PEDOT is the only conducting polymer that is commercially produced on a large-scale and sold worldwide for many applications,[26] such as solid electrolyte capacitors, printed wiring boards, ITO substitution, antistatic coatings, electroluminescent lamps, OLEDs, organic solar cells, electrochromics, organic field-effect transistors, etc. Its monomer, 3,4-ethylenedioxythiophene (EDOT), has been employed as a building block in the design of conjugated systems, which incorporate unique properties such as electrochromic behavior and low band gap polymers.[27,28]

Our continuing interest in polyselenophenes prompted us to improve their optoelectronic properties by designing selenophene-EDOT conjugated systems. Herein, we reported the synthesis and properties of four novel selenophene-EDOT precursors (Scheme 2), and then their electrochemical polymerization, which led to the facile electrodeposition of uniform hybrid selenophene-EDOT polymer films. Finally, the structural characterization, electrochemistry, spectroelectrochemistry, electrochromics, and fluorescence properties of these unique materials, and also structure-property relationship were minutely explored.

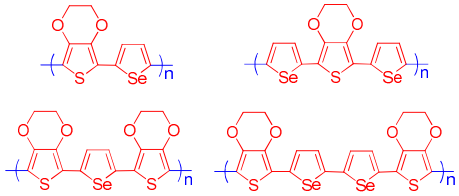

Scheme 2 The designed selenophene-EDOT precursors and their based copolymer materials.

2. Experimental section

2.1 Chemicals

Selenophene (99%; Energy Chemical) and EDOT (98%; Sigma-Aldrich, USA), *N*-bromosuccinimide (NBS, 99%; Energy Chemical), *n*-butyllithium (2.5 mol L^{-1} in hexanes; Energy Chemical), tributylstanny chloride ($SnBu_3Cl$, 98%; Energy Chemical), and tetrakis(triphenylphosphine)palladium(0) [$Pd(PPh_3)_4$, 99%; Energy Chemical] were stored at 4 ºC and used directly without further purification. *N,N*-dimethylformamide (DMF, analytical grade; Beijing East Longshun Chemical Plant), dichloromethane (analytical grade; Beijing East Longshun Chemical Plant), chloroform (>99%; Beijing East Longshun Chemical Plant), and acetonitrile (>99%; Tianjin Bodi Chemicals Co., China) were purified by distillation with calcium hydride under a nitrogen atmosphere before use. Tetrabutyl ammonium hexafluorophosphate (Bu_4NPF_6, 99%; Energy Chemical) was dried under vacuum at 100 ºC for 24 h before use. Tetrahydrofuran (THF) was distilled over Na/benzophenone prior to use. Other chemicals and reagents (analytical grade, >98%) were all purchased commercially from Beijing East Longshun Chemical Plant (Beijing, China) and were used directly without any further treatment.

2.2 Synthesis

2-Bromoselenophene.

N-bromosuccinimide (0.67 g, 3.8 mmol) was added in small amounts into selenophene (0.5 g, 3.8 mmol) in 4 ml of dry dichloromethane and 4 ml acetic acid at 0 °C. The reaction mixture was stirred at 0 °C for 2 h and was washed with deionized water. After drying on $MgSO_4$ and evaporation of solvent, the product was purified by chromatography on silica gel (eluent petroleum ether) to give 2-bromoselenophene as colorless

liquid (0.44 g, 55%). ^{1}H NMR (400 MHz, $CDCl_3$): δ 7.91 (d, 1H), 7.25 (d, 1H), 7.0 (d, 1H).

2,5-Dibromoselenophene.

1.0 g (7.63 mmol) of selenophene and 3.0 g (16.85 mmol) of *N*-bromosuccinimide were dissolved in a solution of 50 mL THF. The solution was stirred at room temperature for 12 h. The solvent was then removed under vacuum by rotary evaporation. The crude product was purified by column chromatography (eluent petroleum ether) to obtain 2.16 g of yellow liquid in 95% yield. ^{1}H NMR (400 MHz, $CDCl_3$): δ 7.0 (d, 2H); ^{13}C NMR (400 MHz, $CDCl_3$): δ 115.61, 132.99.

2,5-Dibromo-3,4-ethylenedioxythiophene.

EDOT (2 g, 14.07 mmol) and *N*-bromosuccinimide (5.5 g, 30.9 mmol) were dissolved in a solution of 50 mL $CHCl_3$ and 50 mL glacial acid. The solution was stirred at room temperature for 2.5 h and poured into 200 mL of distilled water. The organic layer was separated, neutralized with sodium bicarbonate and then filtered. The solvent was removed under vacuum by rotary evaporation. The crude product was purified by column chromatography using $CHCl_3$ as an eluent to obtain 3.63 g of white crystals in 86% yield. ^{1}H NMR (400 MHz, $CDCl_3$): δ 4.26 (s, 4H).

Tributyl(2-selenophenyl)stannane.[29,30]

n-Butyllithium (4.77 mL of a 1.6 M solution in hexane, 7.63 mmol) was added dropwise to selenophene (1 g, 7.63 mmol) in anhydrous THF (10 mL) at -30 °C, and the mixture was stirred at this temperature under argon for 3.5 h. Tributyltin chloride (2.48 g, 7.62 mmol) was added, and the mixture was stirred at -30 °C for further 1 h. Dichloromethane (20 mL) was added and the solution was extracted three times with saturated aqueous sodium carbonate. Organic phase was extracted twice with brine solution, dried over sodium sulfate and solvent was evaporated under vacuum. The residue was further purified by neutral alumina with petroleum ether as the eluent to yield a colorless oil (1.2 g, 75%). ^{1}H NMR (400 MHz, $CDCl_3$): δ 8.35 (d, 1H), 7.5 (m, 2H), 1.6 (m, 6H), 1.31 (m, 6H), 1.08 (t, 6H), 0.91 (t, 9H). ^{13}C NMR (400 MHz, $CDCl_3$): δ 11.12, 13.57, 27.21, 28.93, 130.49, 135.24, 137.85, 143.58.

2-(Tributylstannyl)-3,4-ethylenedioxythiophene.[31]

To a solution containing 2 g (14.07 mmol) EDOT dissolved in 50 mL of dry THF, 6.4 mL (16 mmol) of *n*-butyllithium(2.5 M in hexane) was added dropwise at - 78 °C under argon. After the solution was stirred for 1 h and was warmed to -40 °C, 5.86 g (18 mmol) of tributylstanny chloride was added and the mixture was stirred at the same temperature for 0.5 h before allowing to warm to room temperature. The solvent was removed by rotary evaporation after the solution was stirred for 8 h. The residue was dissolved in hexanes and filtered. The filtrate was dried in vacuum and was used without other purification in the Stille coupling reactions.

2-(Selenophen-2-yl)-3,4-ethylenedioxythiophene.

A 0.4 g (1.9 mmol) sample of 2-bromoselenophene, 3.65 g (5.7 mmol) of 2-(tributylstannyl)-3,4-ethylenedioxythiophene, and 44 mg (2 mol%) of tetrakis(triphenylphosphine)palladium(0) were refluxed in 20 mL of dry DMF for 8 h under argon and poured into 80 mL of distilled water. After extracted with diethyl ether, the organic phase was washed twice with a saturated solution of $NaHCO_3$ then with distilled water. After drying on $MgSO_4$ and evaporation of solvent, the product was purified by chromatography on silica gel (eluent ethyl acetate/petroleum ether) to give 2-(selenophen-2-yl)-3,4-ethylenedioxythiophene as light orange-red solid (0.29 g, 55%). ^{1}H NMR (400 MHz, $CDCl_3$): δ 7.92 (d, 1H), 7.34 (d, 1H), 7.24 (t, 1H); ^{13}C NMR (400 MHz, $CDCl_3$): δ 64.98, 65.43, 97.04, 124.11, 129.5, 137.78, 138.98, 142.18, 143.09, 148.45.

2,5-Di(3,4-ethylenedioxythienyl)-selenophene.

A 0.3 g (1.04 mmol) sample of 2,5-dibromoselenophene, 8.3 g (10.4 mmol) of 2-(tributylstannyl)-3,4-ethylenedioxythiophene, and 0.12 g (10 mol%) of tetrakis(triphenylphosphine)palladium(0) were refluxed in 15 mL of dry DMF for 9 h under argon and poured into 80 mL of distilled water. After extracted with diethyl ether, the organic phase was washed twice with a saturated solution of $NaHCO_3$ then with distilled water. After drying on $MgSO_4$ and evaporation of solvent, the product was purified by chromatography on silica gel (eluent ethyl acetate/petroleum ether) to give 2,5-bis(3,4-ethylenedioxythienyl)-selenophene as orange-red solid (0.34 g, 81%). ^{1}H NMR (400 MHz, $CDCl_3$): δ 7.23 (d, 2H), 6.19 (s, 2H), 4.38 (m, 4H), 4.26 (m, 4H); ^{13}C NMR (400 MHz, $CDCl_3$): δ 65.0, 65.48, 96.92, 115.47, 123.82, 137.49, 137.60, 142.22.

2,5-Diselenophen-2′-yl-3,4-ethylenedioxythiophene.

A 0.4 g (1.3 mmol) sample of 2,5-dibromo-3,4-ethylenedioxythiophene, 1.68 g (3.99 mmol) of tributyl(2-selenophenyl)stannane, and 31 mg (2 mol%) of tetrakis(triphenylphosphine)palladium(0) were refluxed in 20 mL of dry DMF for 10 h under argon and poured into 80 mL of distilled water. After extracted with diethyl ether, the organic phase was washed twice with a saturated solution of $NaHCO_3$ then with distilled water. After drying on $MgSO_4$ and evaporation of solvent, the product was purified by chromatography on silica gel (eluent ethyl acetate/petroleum ether) to give 2,5-diselenophen-2′-yl-3,4-ethylenedioxythiophene as orange-red solid (0.42 g, 78%). ^{1}H NMR (400 MHz, $CDCl_3$): δ 7.94 (d, 2H), 7.35 (d, 2H), 7.24 (t, 2H), 4.42 (m, 4H); ^{13}C NMR (400 MHz, $CDCl_3$): δ 65.43, 124.20, 129.70, 129.79, 137.83, 138.32.

2,2′-Biselenophene.

A 0.8 g (3.8 mmol) sample of 2-bromoselenophene, 4.79 g (11.4 mmol) of tributyl(2-selenophenyl)stannane, and 44 mg (10 mol%) of tetrakis(triphenylphosphine)palladium(0) were refluxed in 20 mL of dry DMF for 8 h under argon and poured into 80 mL of distilled water. After extracted with diethyl ether, the organic phase was washed twice with a saturated solution of $NaHCO_3$ then with distilled water. After drying on $MgSO_4$ and evaporation of solvent, the product was purified by chromatography on silica gel (eluent ethyl acetate/petroleum ether) to give 2,2′-biselenophene as colorless plates (0.51 g, 52%).

5,5'-Dibromo-2,2'-biselenophene.

N-bromosuccinimide (0.68 g, 3.8 mmol) was added in small amounts into 2,2′-biselenophene (0.5 g, 1.9 mmol) in 8 ml of dry dichloromethane at 0 °C. The reaction mixture was stirred at 0 °C for 2 h and was washed with deionized water. After drying on

$MgSO_4$ and evaporation of solvent, the product was purified by chromatography on silica gel (eluent petroleum ether) to give 5.5'-dibromo-2.2'-biselenophene as colorless leaflets (0.31 g, 41%).

5.5'-Di(3,4-ethylenedioxythienyl)-2.2'-biselenophene.

A 0.42 g (1.0 mmol) sample of 5.5'-dibromo-2.2'-biselenophene, 8.3 g (10.4 mmol) of 2-(tributylstannyl)-3,4-ethylenedioxythiophene, and 0.12 g (10 mol%) of tetrakis(triphenylphosphine)palladium(0) were refluxed in 20 mL of dry DMF for 9 h under argon and poured into 80 mL of distilled water. After extracted with diethyl ether, the organic phase was washed twice with a saturated solution of $NaHCO_3$ then with distilled water. After drying on $MgSO_4$ and evaporation of solvent, the product was purified by chromatography on silica gel (eluent ethyl acetate/petroleum ether) to give 5.5'-di(3,4-ethylenedioxythienyl)-2.2'-biselenophene as orange-red solid (0.25 g, 57%). ^{1}H NMR (400 MHz, $CDCl_3$): δ 7.21 (d, 2H), 7.13(d, 2H), 6.21(s,2H), 4.37(m, 4H), 4.27(m, 4H); ^{13}C NMR (400 MHz, $CDCl_3$): δ 64.64, 65.17, 97.0, 114.78, 124.35, 125.78, 137.19, 137.61, 141.89, 142.99.

2.3 Electrosynthesis and electrochemical tests

All electrochemical tests and polymerization were performed in a one-compartment cell with the use of a Model 263A potentiostat-galvanostat (EG&G Princeton Applied Research) under computer control. For electrochemical tests, the working and counter electrodes were typically both Pt wires with a diameter of 1 mm, respectively. To obtain a sufficient amount of the polymer films for characterization, Pt sheet or ITO-coated glass with surface area of 3 cm × 2 cm were employed as the working electrode and another Pt sheet (3 cm × 2 cm) was used as the counter electrode. These aforementioned electrodes were polished carefully with 1500 mesh abrasive paper (for ITO: immersed in ethanol for 6 h and then cleaned by ultrasonic wave for 15 min), cleaned by water and acetone successively, and then dried in air before each experiment. An Ag/AgCl electrode directly immersed in the solution served as the reference electrode, and it revealed sufficient stability during the experiments. The typical electrolytic solution was anhydrous CH_2Cl_2-Bu_4NPF_6 (0.10 mol L^{-1}) containing 0.01 mol L^{-1} oligomers. All the solutions were deaerated by a dry nitrogen stream (more than twenty minutes) and maintained under a slight overpressure through all the experiments to avoid the effect of oxygen.

The polymer film was grown potentiostatically at the optimized potentials higher than the onset oxidation potentials in CH_2Cl_2-Bu_4NPF_6 (0.10 mol L^{-1}), and its thickness was controlled by the total charge passed through the cell, which was read directly from the current-time (I-t) curves by computer. After polymerization, the polymer film was washed repeatedly with anhydrous dichloromethane in order to remove the electrolyte and oligomers. For spectral analyses, the polymer was dedoped chemically with 25% ammonia for three days and washed repeatedly with neat water to exclude the dopants. Finally, the polymer was dried at 60 °C under vacuum for 24 h.

2.4 Characterization

Electrochemical, spectroelectrochemical and kinetic studies were carried out on a Model 263 potentiostat-galvanostat (EG&G Princeton Applied Research) and a Cary 50 UV-vis-NIR spectrophotometer under computer control. Infrared spectra were determined with a Bruker Vertex 70 Fourier-transform infrared (FT-IR) spectrometer with samples in KBr pellets. UV-vis spectra of the soluble part of the as-formed hybrid polymers dissolved in DMSO were taken by using Perkin-Elmer Lambda 900 ultraviolet-visible near-infrared spectrophotometer. With an F-4500 fluorescence spectrophotometer (Hitachi), the fluorescence spectra of the oligomers and soluble part of the copolymers were determined in DMSO. Scanning electron microscopy (SEM) measurements were made by using a VEGA II-LSU scanning electron microscope (Tescan) with the polymer deposited on the indium-tin-oxide (ITO) coated glass.

Spectroelectrochemical measurements were carried out to consider absorption spectra of the hybrid polymers film under the applied potential. The spectroelectrochemical cell consists of a quartz cell, an Ag wire, a Pt wire, and an ITO/glass as the transparent working electrode. All measurements were carried out in oligomer-free CH_2Cl_2-Bu_4NPF_6 (0.10 mol L^{-1}). It should be noted here that the quartz cell filled with oligomer-free CH_2Cl_2-Bu_4NPF_6 (0.10 mol L^{-1}) and ITO-coated glass without deposited film was used as the background for spectroelectrochemical measurements.

The change in optical density (ΔOD) at a specific wavelength (λ_{max}) was determined by $\%T$ values of electrochemically oxidized and neutral films, using the equation (1):[32]

$$\Delta OD = \log(T_{ox}/T_{red}) \quad (1)$$

The coloration efficiency (CE) is defined as the relation between the injected/ejected charge as a function of electrode area (Q_d) and the change in optical density (ΔOD) at a specific dominant wavelength (λ_{max}) as illustrated by the following equation (2):[33]

$$CE = \Delta OD/Q_d \quad (2)$$

2.5 *Details of Computations*

All calculations were carried out using the Gaussian 03 program.[34] The structure of the oligomers were optimized without symmetry constraints using a hybrid density functional[35,36] and Becke's threeparameter exchange functional combined with the LYP correlation functional (B3LYP)[37,38] and with the 6-31G(d,p) basis set (B3LYP/6-31G(d,p)). Vibrational frequencies were evaluated at the same level to identify the real minimal energy structures.

3. Results and Discussion

3.1 Oligomer synthesis

We adopted an iterative divergent method for the synthesis of these Se-EDOT oligomers, as shown in Scheme 3. The intermediate products including 2-bromoselenophene, 2,5-dibromoselenophene, tributyl(selenophene-2-yl)stannane and tributyl(2,3-dihydrothieno[3,4-b][1,4]dioxin-5-yl)stannane[32,33] were synthesized with moderate/high yields. 2,5-Dibromo-3,4-ethylenedioxythiophene was achieved by addition of 1.2 equimolar *N*-bromosuccinimide (NBS) into the

mixture of EDOT and DMF, and importantly, the reaction must be kept in dark place. Lastly, a convenient method for the formation of carbon-carbon bond, Stille coupling reaction, was first used to combine EDOT and selenophene unit to give the target compounds in satisfactory yields (typically more than 70%). Importantly, the hybrid Se-EDOT oligomers were synthesized and their properties were investigated for the first time as we known. ^{1}H and ^{13}C NMR spectra of some intermediates and target compounds are displayed in Figure S1~S12.

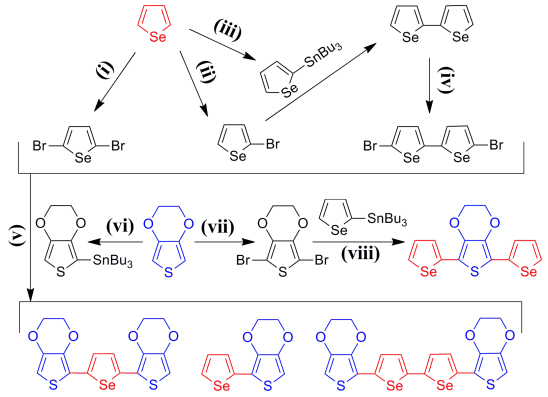

Scheme 3 Synthetic route of Se-EDOT oligomers. Reagents and conditions: (i) NBS (2.2 eq), THF, RT; (ii) NBS (1 eq), CH_3COOH/CH_2Cl_2, 0 °C; (iii) *n*-BuLi, $SnBu_3Cl$, THF, -30 °C; (iv) NBS (2 eq), CH_2Cl_2, 0 °C; (v) $Pd(PPh_3)_4$, refluxing DMF; (vi) *n*-BuLi, THF, -78 °C, then $SnBu_3Cl$, -40 °C; (vii) NBS (2.2 eq), $CH_3COOH/CHCl_3$, RT; (viii) $Pd(PPh_3)_4$, refluxing DMF.

3.2 Electrochemical polymerization of Se-EDOT oligomers

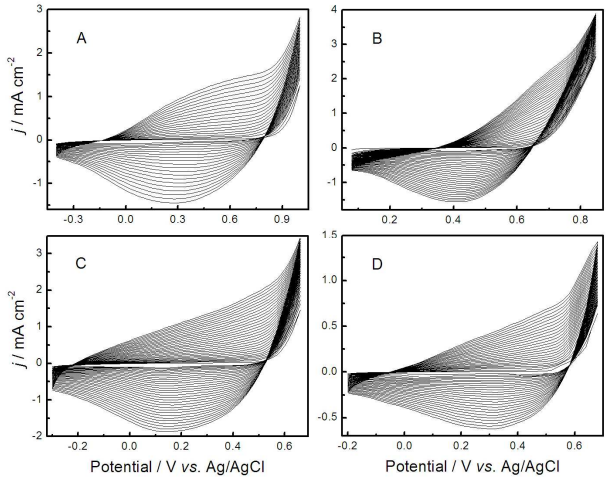

Figure 1 Cyclic voltammograms (CVs) of the electropolymerization of 0.01 mol L^{-1} Se-EDOT (A), Se-EDOT-Se (B), EDOT-Se-EDOT (C), and EDOT-Se-Se-EDOT (D) on a Pt working electrode in CH_2Cl_2-Bu_4NPF_6 (0.10 mol L^{-1}). Potential scan rate: 100 mV s^{-1}.

The electropolymerization performances of these oligomers were examined in CH_2Cl_2-Bu_4NPF_6 (0.10 mol L^{-1}) system. From their anodic oxidation behavior (see Figure S13), the oxidation of Se-EDOT was initiated at 0.89 V, while with the elongation of π-conjugated chain length, the onset oxidation potentials of Se-EDOT-Se, EDOT-Se-EDOT, and EDOT-Se-Se-EDOT were further brought down to 0.66, 0.55, and 0.53 V, respectively. Also, by employing EDOT as the terminal groups (EDOT-Se-EDOT), the oligomer is easier to be oxidized than in the case of Se as ending groups (Se-EDOT-Se). These values are significantly lower than those of selenophene and EDOT due to the elongation of conjugated systems.

Figure 1 shows the CVs corresponding to the potentiodynamic electropolymerization of four Se-EDOT oligomers. Application of repetitive potential scans between -0.5 V and the foot of the oxidation wave of the precursor results in the development of a broad redox system in the region of -0.3~0.80 V corresponding to the oxidation and subsequent reduction of the oxidized polymer. Visual inspection during CV experiments revealed the formation of compact and homogeneous polymer films on the electrode surface. The increase of anodic and cathodic peak current densities in CVs implied that the amount of the polymer film increased on the electrode surface. The broad redox waves of the polymer may be ascribed to the wide distribution of polymer chain length or the conversion of conductive species on the polymer main chain from the neutral state to the metallic state. The potential shift of current density peaks provided information about the increase in the electrical resistance of the polymer film and the overpotential needed to overcome this resistance. This behavior shows characteristic features of conducting polymers during potentiodynamic synthesis, also in full agreement with selenophene[1,11,12] and EDOT[26].

3.3 Optimization of electrical conditions and preparation of the hybrid polymers

Potentiostatic electrolysis was employed to prepare the polymer film for characterization. To optimize the applied potential for polymerization, a set of current transients during the electropolymerization at different applied potentials were recorded, as shown in Figure S14. Typically, at applied potentials below the onset oxidation potential, no polymer film was found on the electrode, indicating that polymerization does not occur on the electrode surface due to the low resultant current density. Once the applied potential reaches the threshold value, all the electrosynthetic current densities initially experience a sharp increase and then a slow decrease and finally keep constant as a result of uniform deposition of the polymer film on the electrode surface. However, at relatively high potentials, the surfaces of the polymer films became rough, discontinuous, and heterogeneous. Worsely, during/after the experiments, some film even fell down into the solution from the electrode surface. This phenomenon was mainly due to the significant overoxidation at higher potentials, which led to poor quality films. Considering the overall factors affecting the quality of the formed film, such as moderate polymerization rate, negligible overoxidation, regular morphology, and good adherence against the working electrode, the optimized polymerization potentials for Se-EDOT, Se-EDOT-Se, EDOT-Se-EDOT, and EDOT-Se-Se-EDOT are 0.95, 0.85, 0.70, and 0.60 V *vs.* Ag/AgCl, respectively. Therefore, the polymer films used for the characterization mentioned below were all prepared by the chronoamperometry method at these constant potentials in CH_2Cl_2-Bu_4NPF_6 (0.10 mol L^{-1}).

3.4 Structural characterization

FT-IR spectra of the oligomers and the corresponding neutral polymers were recorded to elucidate their structure and interpret the polymerization mechanism, as shown in Figure 2. For all polymers, the bands due to C_{α}-H stretching at about 3106 cm^{-1} and C_{β}-H stretching at 3047 cm^{-1} in the spectra of the oligomers are nearly absent/become weak, while those in the region of 3000-2800 cm^{-1} remain in the spectra, indicating the occurrence of electropolymerization at the thiophene/selenophene rings. In the fingerprint region, the immergence of the characteristic peaks at around 843~836 cm^{-1} could be assigned to the out-of-plane bending vibration of adjacent C-H in the thiophene/selenophene ring, which confirms the polymerization mainly occurs at α-positions, namely, $C_{(2)}$ and $C_{(5)}$ positions, in good agreement with the results previously reported.[11,12]

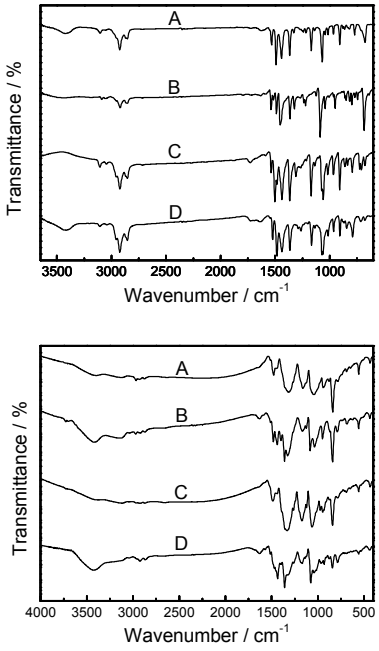

Figure 2 FT-IR spectra of the oligomers (upper panel) and the hybrid polymers (lower panel). Left: Se-EDOT (A), Se-EDOT-Se (B), EDOT-Se-EDOT (C), and EDOT-Se-Se-EDOT (D). Right: PSe-EDOT (A), PSe-EDOT-Se (B), PEDOT-Se-EDOT (C), and PEDOT-Se-Se-EDOT (D).

As can be seen from the figure, the absorption bands in the spectra of the hybrid polymers were obviously broadened in comparison with those of the oligomers, similar to those of other conducting polymers reported previously.[11,12,39,40] This instance was probably due to the resulting product composed of oligomers/polymers with wide chain dispersity. In more detail, the vibrational modes of the polymers with different polymerization degrees show different IR shifts. These peaks overlapped one another and produced broad bands with hyperstructures. Furthermore, the chemical defects on the polymer chains resulting from the overoxidation of the polymer and α-β, β-β connections also contributed to the band broadening of IR spectra.

3.5 Computational results

Quantum chemical calculations can be applied effectively in the search for the structural study of newly obtained compounds and polymers. Optimized ground-state geometries of all the oligomers have been obtained at the B3LYP/6-31G* level (Figure S15). The optimized dihedral angles between the thiophene ring and selenophene units are summarized in Table 1. One can see that all oligomers show very planar structures (close to 180°, Table 1 and Figure S15), indicating the highest possible π-electron coupling, which is very beneficial to lower the HOMO-LUMO gap of the corresponding polymers and to prepare conjugated polymers with enhanced main chain planarity and higher electrical conductivity. Note here that the ground-state geometry of EDOT-Se-Se-EDOT is slightly more twisted than the others, but it is still less twisted than BisEDOT-2,2′-bithiophene units (168°). From this point, the selenophene units could be considered in the rational design of planar π-conjugated systems.

Table 1 The calculated and experimental parameters of Se-EDOT oligomers

Compounds	Dihedral angles (deg)	HOMO (eV)	LUMO (eV)	HOMO-LUMO gap (eV)	$E_{ox,onset}$ (V)	$E_{g,opt}$ (eV)	$\lambda_{abs,max}$ (nm)	$\lambda_{em,max}$ (nm)
Se-EDOT	179	-5.40	-1.42	3.98	0.89	3.49	325	316
Se-EDOT-Se	179, 179	-5.09	-1.86	3.23	0.66	2.92	380	450
EDOT-Se-EDOT	179, 179	-4.91	-1.66	3.24	0.55	2.58	380	451
EDOT-Se-Se-EDOT	179, 176, 179	-4.81	-1.99	2.82	0.53	2.48	425	520

During the electropolymerization, a necessary step is that the oxidation reaction leads to the ionization of molecules and to the formation of a radical cation. The polymerization is believed to proceed through the α positions of the external heterocylic rings like thiophene and selenophene. Those atoms with a negative Mulliken charge will donate electrons during electrochemical polymerization and reactions between radical cations mainly occur on the frontier molecular orbital according to the molecular orbital theory. For all the molecules, the negative electric charges mainly concentrated on C-H bonds (Figure S16: the calculated Mulliken charge of these oligomers). However, no significant difference was observed between the calculated Mulliken charges of α and β sites on the thiophene/selenophene rings. The calculated molecular orbitals of these oligomers demonstrated that the HOMO proportions for α sites were higher than those of other atoms (Figure 3). On the other hand, there was steric hindrance on the β sites of EDOT-Se-EDOT and EDOT-Se-Se-EDOT. Based on these results, it can be reasonably deduced that the polymerization sites of these compounds are preferentially α positions.

The electron density distribution in the cations governs the electron spin density (ESD), which is believed to be the main factor controlling the polymerization. In this context, the most likely coupling sites are believed to be those with the highest ESD. From the calculated atomic ESD distribution in the radical cations (Figure 3), it can be seen that the central rings and the external

rings donated almost equally to the ESD distribution. Due to their privileged position with few steric obstacles, the α-carbon of external rings constitutes a site for electropolymerization. Also, from Figure 3, the highest unpaired ESDs are obviously all located at the α positions (α-carbon) in the external rings. These calculations further confirmed the deduction mentioned previously and the polymerization of these oligomers would happen dominantly at α positions. But it should be noted here that the delocalization of the charge on the extended structures influences their chemical reactivity because of the significant stabilization of the formed species. As the chain length increases, ESD on the α positions decreases, but not as much as the HOMO proportion. Namely, the stability of the corresponding radical cations increases, also leading to a decrease of polymerizability and thus α-β, β-β connections in the cases of Se-EDOT and Se-EDOT-Se.

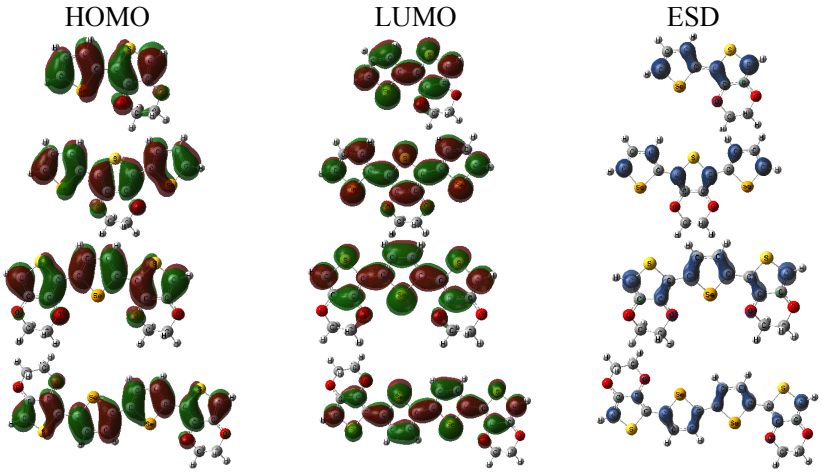

Figure 3 HOMO and LUMO orbitals of Se-EDOT oligomers and isovalent surfaces (0.01 electron/bohr3) of electron spin densities (in blue) for their radical cations.

3.6 Morphology

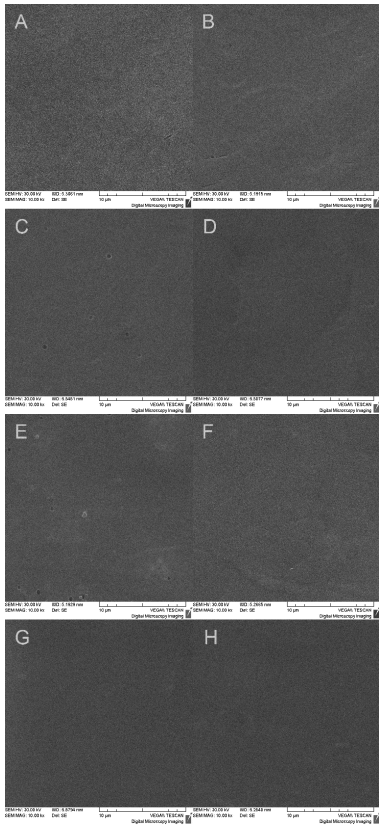

Figure 4 SEM images of the hybrid polymer films deposited electrochemically on the ITO electrode for 100 s. Magnification: 10 000×. A, C, E, G: doped PSe-EDOT, PSe-EDOT-Se, PEDOT-Se-EDOT and PEDOT-Se-Se-EDOT; B, D, F, H: dedoped PSe-EDOT, PSe-EDOT-Se, PEDOT-Se-EDOT and PEDOT-Se-Se-EDOT, respectively.

Surface morphologies of conducting polymers are closely related to their properties, such as electrical conductivity, redox activity and stability, etc. Therefore, the surface of the doped polymer films deposited electrochemically on the ITO electrode (the average thickness of the hybrid polymer films in the range of 180~210 nm) was observed by scanning electron microscope (SEM), as shown in Figure 4. Macroscopically, all the polymer films appeared to be smooth and homogeneous. Microscopically, even at high magnifications (10 000×), the surfaces of the doped polymer films (Figure 4, the left column) are still rather smooth and continuous with few defects. After dedoping at a negative constant applied potential (-0.4 V), the morphology of the polymer film showed no obvious difference (Figure 4, the right column), implying that the dedoping processes did not destroy the surface morphologies of the doped polymers. The morphology of compact polymer films were extremely beneficial to improve their electrical conductivity and electron transfer capability and also make them good candidates for applications in ion-selective electrodes, ion-sieving films, and matrix for hosting catalyst particles, etc.[41,42]

3.7 Solubility, electrical conductivity, UV-vis and fluorescence spectra of oligomers and polymers

The oligomers show good solubility in conventional organic solvents, while the electropolymerized polymer films can partly dissolve in strong polar solvents at room temperature, such as DMSO, NMP, acetonitrile, THF. The poor solubility of the

hybrid polymers are probably due to their longer polymer chain sequences after polymerization. Further, cross-linking of polymer chains through β-defects would also cause these polymers to be insoluble.

The hybrid polymer films in doped states were directly obtained via electropolymerization and their electrical conductivity was determined to be in the range of 10^{-1}~10^{1} S cm^{-1} by applying a conventional four-probe technique, intermediate between electrodeposited polyselenophene (10^{-4}~10^{-2} S cm^{-1})[1] and PEDOT (10^{0}~10^{2} S cm^{-1})[26]. Post-processing by using strong polar solvents could improve their conductivity. The detailed information, together with their thermoelectric performances, will be reported elsewhere.

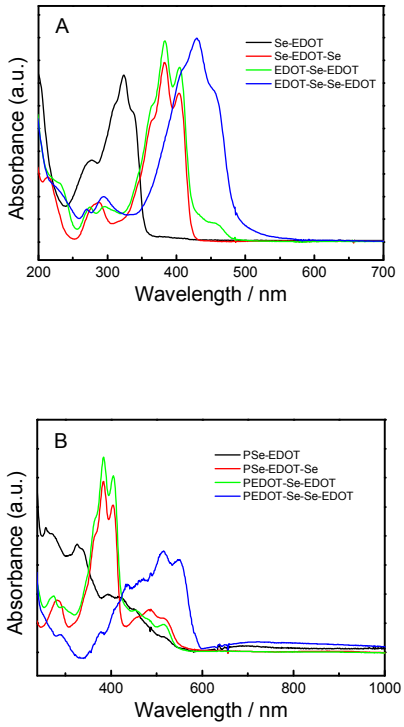

Figure 5 UV-vis spectra of the oligomers (A) and the soluble part of hybrid polymers (B). Solvent: acetonitrile.

UV–vis spectra of both the oligomers and the soluble part of hybrid polymers were examined in solvents, as shown in Figure 5. The oligomers show similar characteristic π–π* transition peaks in the region of 300~500 nm (Figure 5 A and Table 1) with optical band gap from 3.49 to 2.48 eV. These values are all lower than the calculated results, probably due to the solvation effect and stronger intermolecular interactions due to the introduction of selenophene units (including Se-Se, S-O, Se-S, Se-O interactions). With the elongation of π-conjugated systems, significant red shift could be observed from Se-EDOT to EDOT-Se-EDOT/Se-EDOT-Se (about 55 nm) and further to EDOT-Se-Se-EDOT (about 45 nm) (Figure 5 B). Due to the further increase in the conjugated chain length, the overall absorption of the polymers tailed off to 550~600 nm (Figure 5 B and Table 2) in comparison with those of the oligomers (355~500 nm), and might be more for the insoluble part due to their longer chain length. These spectral results confirmed the occurrence of electrochemical polymerization among the oligomers and the formation of a conjugated polymer.

The fluorescence emission spectra of the oligomers and the dedoped polymers were determined in acetonitrile, as shown in Figure 6. In agreement with the UV-vis spectral results, the emission spectra of the oligomers displayed significant red shifts with the elongation of π-conjugated systems (emission peaks from 320 nm to 520 nm, Table 1). The fluorescence quantum yields ($\phi_{overall}$) was calculated to be 0.015, 0.05, 0.03, and for Se-EDOT, Se-EDOT-Se, and EDOT-Se-EDOT, respectively, according to the procedure in our previous reports.[39,43-45] EDOT-Se-Se-EDOT exhibits the highest quantum yield of 0.09, but is still lower than that of the thiophene analogue (0.17). Obvious red shifts could be observed between the oligomers and the soluble polymers from the figure, which is mainly attributable to the elongation of the polymer's delocalized π–electron chain sequence.

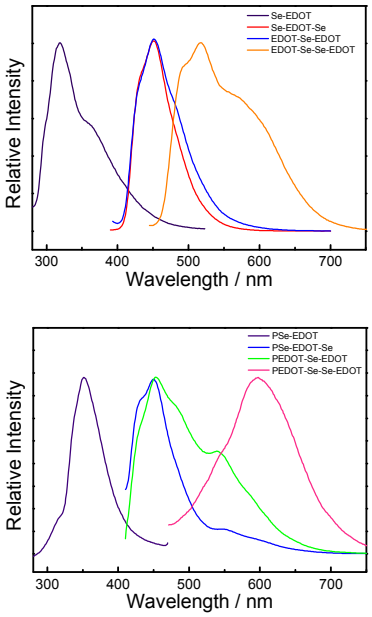

Figure 6 Fluorescence spectra of the oligomers and the polymers in acetonitrile as indicated and photoluminescence of the oligomers in dichloromethane under 365 nm UV irradiation (Left to right: Se-EDOT, Se-EDOT-Se, EDOT-Se-EDOT and EDOT-Se-Se-EDOT).

Meanwhile, it is also very interesting to find that the oligomers dissolved in common organic solvents, such as methanol, ethanol, acetone, acetonitrile, diethyl ether, DMSO, can all emit blue to orange-yellow photoluminescence when exposed to 365 nm UV light, as shown in Figure 6, whereas the soluble polymers showed no emissions as in the cases of polyselenophene and PEDOT.

From these results, all the oligomers and the hybrid polymer films show unsatisfied fluorescence properties except the case of EDOT-Se-Se-EDOT, which displays orange-yellow photoluminescence with a relatively high quantum yield. As a orange-yellow fluorophore, it probably should be considered in the rational design of highly fluorescent π-conjugated materials.

Table 2 The properties of the hybrid Se-EDOT polymers

polymers	electrochemistry and linear fitting				redox stability		absorption		$E_{g,opt}$ (eV)
	$E_{ox,peak}$ (V)	$E_{red,peak}$ (V)	R^2_{an}	R^2_{cat}	10000th	50000th	λ_{onset} (nm)	λ_{max} (nm)	
PSe-EDOT	0.73	0.42	0.9994	0.9985	73.8%	-	745	565	1.66
PSe-EDOT-Se	0.79	0.58	0.9976	0.9948	82.6%	-	709	526	1.75
PEDOT-Se-EDOT	0.53	0.30	0.9994	0.9990	100.3%	72.9%	769	528	1.61
PEDOT-Se-Se-EDOT	0.70	0.52	0.9984	0.9990	85.5%	62.4%	806	601	1.54

3.8 Electrochemistry of the hybrid polymers

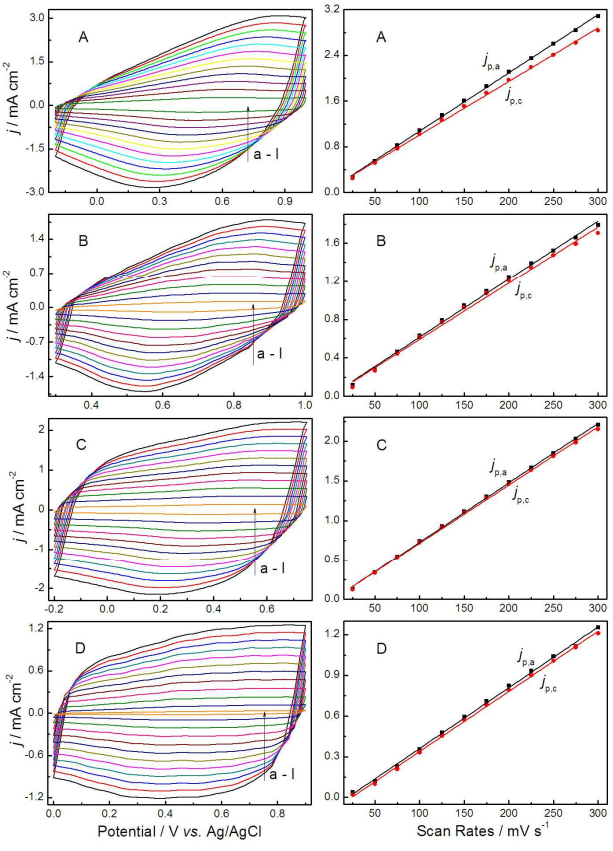

Figure 7 Cyclic voltammograms (CVs, right column) of PSe-EDOT (A), PSe-EDOT-Se (B), PEDOT-Se-EDOT (C), and PEDOT-Se-Se-EDOT (D) modified Pt electrodes in oligomer-free CH_2Cl_2-Bu_4NPF_6 (0.10 mol L^{-1}) at potential scan rates of 300 (a), 275 (b), 250 (c), 225 (d), 200 (e), 175 (f), 150 (g), 125 (h), 100 (i), 75 (j), 50 (k), and 25 (l) mV s^{-1}. Left: plots of redox peak current densities *vs*. potential scan rates. j_p is the peak current density, and $j_{p,a}$ and $j_{p,c}$ denote the anodic and cathodic peak current densities, respectively. The hybrid polymer films were deposited electrochemically on Pt electrode under optimal potentials for 50 s and the average thickness of the hybrid polymer films are determined to be in the range of 90~110 nm.

The electrochemical behaviors of the polymers-modified Pt electrodes were studied by cyclic voltammetry in oligomer-free electrolytes to test their electroactivity and stability. The CVs of the polymers under different potential scan rates represented broad anodic and cathodic peaks similar with those of polyselenophene and PEDOT. All the peak current densities were proportional to potential scanning rates (left column of Figure 7 and Table 2), indicating that the redox process is non-diffusional and electroactive materials are well adhered to the working electrode surface. Furthermore, CVs of all the polymers in oligomer-free electrolytes (Figure 7) showed an obvious hysteresis, *i. e.*, an obvious difference between the anodic and cathodic peak potentials.[46,47] The potential shift of redox peaks among CV curves for conducting polymers is hardly explained by conventional kinetic limitations such as ion diffusion or interfacial charge transfer processes. The main reasons accounting for this phenomenon are usually as follows, slow heterogeneous electron transfer, local rearrangement effect of polymer chains, slow mutual transformation of various electronic species, and electronic charging of interfacial exchange corresponding to the metal/polymer and polymer/solution interfaces, etc.[46] It is also found that as the ratio of selenophene units decreasing and EDOT increasing, the hybrid Se-EDOT polymers display lower oxidation and reduction potentials with better linear fitting of peak current densities, as shown in Table 2, tending to the unique properties of PEDOT[26] and compensating for polyselenophene.

It is well known that the good stability of conducting polymers is very significant for their applications in electronic devices.[48] For example, the long-term stability upon switching and/or cycling plays a key role on the electrochromic performance of the devices and smart windows. For that reason, the long-term stability of these polymer films, which were deposited on Pt

electrode, upon cycling was elaborated by potential scanning between neutral and oxidized states in oligomer-free CH_2Cl_2-Bu_4NPF_6 (0.10 mol L^{-1}) at the potential scan rate of 150 mV s^{-1}, as shown in Figure 8. It was noted that all the polymer films exhibited outstanding stability retaining at least 73% of the electroactivity even after 10 000 cycles (see Table 2). PEDOT-Se-EDOT and PEDOT-Se-Se-EDOT displayed even better stability with the amount of exchange charge still remaining ~73% and 62% after sweeping 50 000 cycles, respectively. Note here that the stability tests were carried out under an air atmosphere and the imposed conditions were not very stringent. If they were sealed in fabricated devices, the long-term stability of these materials upon switching and/or cycling would be further increased. These results indicated outstanding redox stability of the hybrid polymer materials, much better than polyselenophene[1] and even competitive with PEDOT.[26] Also, as highly stable electroactive materials, they probably find applications in various fields, such as electrochromics, supercapacitors, electrochemical (bio)sensors.

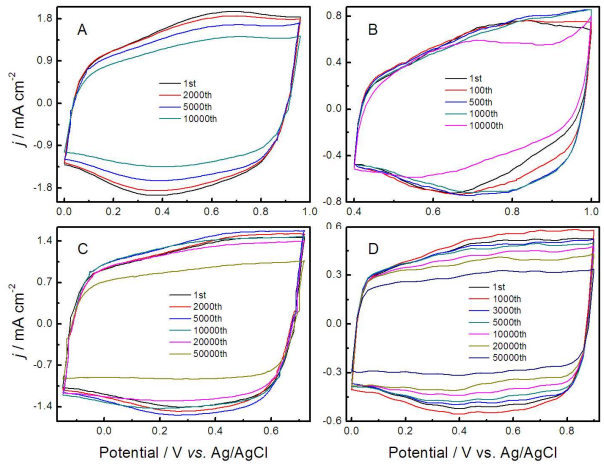

Figure 8 Long-term cyclic voltammograms of the polymers in oligomer-free CH_2Cl_2-Bu_4NPF_6 (0.10 mol L^{-1}). Potential scan rate: 150 mV s^{-1}. PSe-EDOT: (A), PSe-EDOT-Se: (B), PEDOT-Se-EDOT: (C), and PEDOT-Se-Se-EDOT: (D). The hybrid polymer films were deposited electrochemically on Pt electrode under optimal potentials for 50 s and the average thickness of the hybrid polymer films are determined to be in the range of 90~110 nm.

3.9 Spectroelectrochemistry

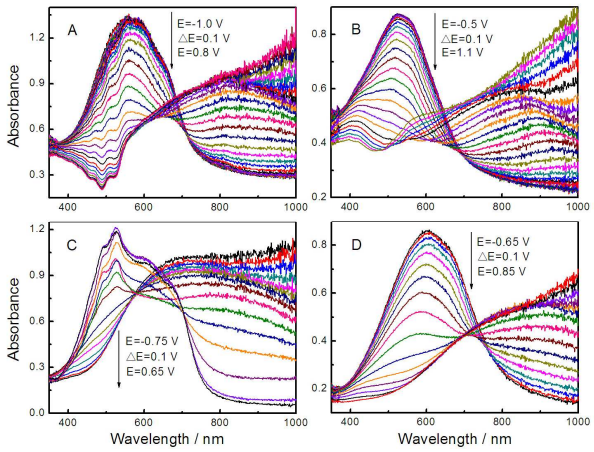

Figure 9 Spectroelectrochemistry for the hybrid polymer films on the ITO coated glass in oligomer-free CH_2Cl_2-Bu_4NPF_6 (0.10 mol L^{-1}) solution between the potentials indicated (ΔE = 0.1 V). PSe-EDOT: (A), PSe-EDOT-Se: (B), PEDOT-Se-EDOT: (C), and PEDOT-Se-Se-EDOT: (D). The hybrid polymer films were deposited electrochemically on Pt electrode under optimal potentials for 200 s and the average thickness of the hybrid polymer films are all around 350~380 nm.

For the viewpoint of device and high-performance display applications, spectroelectrochemical properties of the electrochromes should be manifested by using the changes in optical absorption spectra under voltage pulses. Therefore, UV-vis spectra of the hybrid polymers that were electrodeposited on ITO-coated glass slides via potential cycling were recorded *in situ* in oligomer-free CH_2Cl_2-Bu_4NPF_6 (0.10 mol L^{-1}) after neutralization (Figure 9). The potential applied to the polymer-coated electrode was initially in the fully reduced state and then sequentially increased to higher potentials to oxidize the polymer while monitoring the creation of the charge carriers.

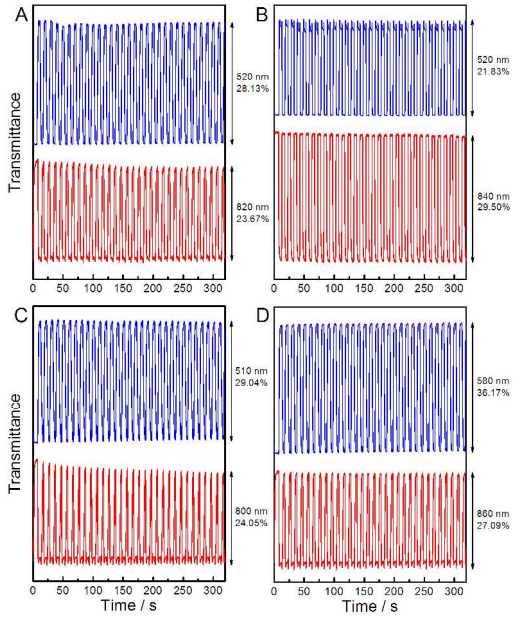

Figure 10 Transmittance-time profiles of the hybrid polymer films recorded during double step spectrochronoamperometry for the switching time of 10 s under the indicated wavelength. A: PSe-EDOT between -1.0~0.8 V; B: PSe-EDOT-Se between -0.5~1.1 V; C: PEDOT-Se-PEDOT between -0.75~0.65 V; D: PEDOT-Se-Se-PEDOT between -0.65~0.85 V.

Similar to PEDOT or polyselenophene, a dominant absorption with the maximum at around 500~600 nm characterized the spectrum for all the dedoped hybrid polymers. However, there are several fine structures for PSe-EDOT in the range of 450~550 nm, probably caused by structural randomness (Se-EDOT/Se-Se couplings) and irregularity (α,β-coupling) during electropolymerization. The band gap (E_g) of the hybrid polymers were calculated from the onset of the low energy end of π-π* transitions to be 1.66 (PSe-EDOT, 745 nm), 1.75 (PSe-EDOT-Se, 709 nm), 1.61 (PEDOT-Se-EDOT, 769 nm), and 1.54 eV (PEDOT-Se-Se-EDOT, 806 nm), respectively. It can be easily concluded that the smallest band gap can be obtained when EDOT units were attached as the terminal part to selenophene/biselenophene, probably because of their well-defined structures with less defects in the main chain. On the other hand, the E_g for PEDOT-Se-EDOT and PEDOT-Se-Se-EDOT is same to or even lower than PEDOT (~1.6 eV)[27], which is probably due to the more effective intramolecular charge transfer between EDOT and selenophene units (HOMO-LUMO interaction).

Upon oxidation, the intensity of the absorption bands started to decrease simultaneously with a concomitant increase in the near-IR region, representing the formation of polaronic (at around 820 nm) and bipolaronic (more than 900 nm) bands.[27] These changes in the absorption spectra were accompanied with color changes from purplish, reddish and saturated blue in the reduced form to transmissive sky blue/green (close to colorless) states during the *p*-doping process (see Table S1). The color change from one to a highly transmissive state, as in cases of these hybrid polymers, is also a quite significant trait in RGB polymer electrochromics and especially useful in display applications.

3.10 *Electrochromic properties*

The optical switching studies of the hybrid polymer films were carried out using a square wave potential step method coupling with optical spectroscopy known as chronoabsorptometry in oligomer-free CH_2Cl_2-Bu_4NPF_6 (0.10 mol L^{-1}) solution. The electrochromic parameters, such as optical contrast ratio (Δ*T*%) and response time, were investigated by increment and decrement in the transmittance with respect to time at the specific absorption wavelengths, as shown in Figure 10. The potentials were switching alternatively between the reduced and oxidized states with the residence time of 10 s. Electrochromic parameters of all the hybrid polymer films are summarized in Table 3. All the hybrid polymers displayed moderate to excellent transmittance ratios in the range of 22~36% at different wavelengths and decent coloration efficiency (CE) values (at 95% of the full contrast, see Table 3). Among them, PEDOT-Se-EDOT and PEDOT-Se-Se-EDOT showed relatively high CE values (187 and 203 cm^2 C^{-1}), even higher when compared to PEDOT (137 cm^2 C^{-1})[27]. Also, these polymers switch rapidly between their neutral and oxidized states. PSe-EDOT-Se revealed impressive switching times of 0.5 s at 520 nm and 0.7 s at 840 nm to achieve 95% of their optical contrasts for the dedoping process. No more than 1 s is required for PEDOT-Se-EDOT and PEDOT-Se-Se-EDOT films. Note that these values are among the best ones.[27]

Table 3 Electrochromic parameters of the hybrid polymers at different wavelengths

sample	wavelength (nm)	T_{red}	T_{ox}	Δ*T*	response time (s)		coloration efficiency (cm^2/C)
					ox	red	
PSe-EDOT	520	5.7%	33.8%	28.1%	2.9	2.1	108.1
	820	35.3%	11.6%	23.7%	1.3	2.1	83.3
PSe-EDOT-Se	520	11.1%	33.2%	22.1%	1.2	0.5	102.6
	840	47.5%	18.0%	29.5%	1.7	0.7	133.4
PEDOT-Se-PEDOT	510	13.1%	42.1%	29.0%	2.6	3.2	186.9
	800	41.6%	17.5%	24.1%	0.9	2.8	154.8
PEDOT-Se-Se-PEDOT	580	12.6%	49.1%	36.5%	2.3	3.0	203.2
	860	51.1%	24.0%	27.1%	0.9	2.1	118.7

The stability and color persistence is another important feature for the application of electrochromic materials because it is directly related to aspects involved in its utilization and energy consumption during that utilization. The optical stability was controlled by using a square wave potential step method together with measuring its spectra. As shown in Figure S17, after 100 cycles of operation, the optical activity of these polymers was preserved up to more than 95%, in good agreement with CV results.

4. Conclusions

In this paper, four novel selenophene-EDOT oligomers were synthesized and their electrochemical polymerization in CH_2Cl_2-Bu_4NPF_6 (0.10 mol L^{-1}) was reported. The structure-property relationships of the oligomers and the electrosynthesized hybrid polymers, including structure characterization, electrochemical, electronic and optical properties, quantum chemistry calculations and morphology, were systematically investigated. It is found that all the oligomers show planar structure and blue to orange-yellow photoluminescence, and these units probably should be considered in the rational design of π-conjugated materials with high fluorescence and/or enhanced main chain planarity. Also, low oxidation potentials led

to the facile deposition of uniform hybrid polymer films with outstanding electroactivity and stability suffice for various applications. Electrochromic and kinetic studies demonstrated that the hybrid polymers revealed high contrast ratios, favorable coloration efficiencies, low switching voltages, fast response time, excellent stability and color persistence, which provides more plentiful electrochromic colors and holds promise for display applications. Overall, the obtained hybrid polymers featured the advantageous combination of polyselenophene and PEDOT, such as lower band gap and better planarity of polyselenophene, high conductivity, transparency and excellent stability of PEDOT. This method, to design the hybrid polymers of selenophenes with other units, could probably be an effective way to overcome the disadvantages and retain the superiority of polyselenophenes, and a portfolio of these materials hold promise for the design of a new generation of optoelectronic materials and may find application in electrochemical sensors and organic electronic devices.

Acknowledgement

We are grateful to the National Natural Science Foundation of China (grant number 51303073), the Natural Science Foundation of Jiangxi Province (grant numbers 20122BAB216011), Ganpo Outstanding Talents 555 projects (2013), the Training Plan for the Main Subject of Academic Leaders of Jiangxi Province (2011), and the Science and Technology Landing Plan of Universities in Jiangxi province (KJLD12081) for their financial support of this work. Thanks are also due to Prof. Dr. Guangming Nie in Qingdao Science and Technology University for his kind assistance on the electrochromic tests, and Dr. Yuzhen Li in Fudan University for her kind assistance on the quantum chemistry calculations.

Supporting Information

^{1}H and ^{13}C NMR spectra of all the intermediates and target compounds; anodic oxidation and chronoamperometric curves, optimized structures, and main atomic electron density populations of the oligomers; switching colors from doped to dedoped states and optical stability tests upon repeated cycling of the hybrid polymers.

References

1 Patra, A.; Bendikov, M. *J. Mater. Chem.* **2010**, *20*, 422–433 and references therein.
2 Zade, S. S.; Zamoshchik, N.; Bendikov, M. *Acc. Chem. Res.* **2011**, *44*, 14–24.
3 Patra, A.; Wijsboom, Y. H.; Zade, S. S.; Li, M.; Sheynin, Y.; Leitus, G.; Bendikov, M. *J. Am. Chem. Soc.* **2008**, *130*, 6734–6736.
4 Wijsboom, Y. H.; Patra, A.; Zade, S. S.; Li, M.; Sheynin, Y.; Shimon, L. J. W.; Bendikov, M. *Angew. Chem., Int. Ed.* **2009**, *48*, 5443–5447.
5 Li, M.; Patra, A.; Sheynin, Y.; Bendikov, M. *Adv. Mater.* **2009**, *21*, 1707–1711.
6 Li, M.; Sheynin, Y.; Patra, A.; Bendikov, M. *Chem. Mater.* **2009**, *21*, 2482–2448.
7 Patra, A.; Wijsboom, Y. H.; Leitus, G.; Bendikov, M. *Chem. Mater.* **2011**, *23*, 896–906.
8 Saadeh, H. A.; Lu, L.Y.; He, F.; Bullock, J. E.; Wang, W.; Carsten, B.; Yu, L.P. *ACS Macro Lett.* **2012**, *1*, 361–365.
9 Kronemeijer, A.; Gili, J. E.; Shahid, M.; Rivnay, J.; Salleo, A.; Heeney, M.; Sirringhaus, H. *Adv. Mater.* **2012**, *24*, 1558–1565.
10 Chen, Z. Y.; Lemke, H.; Albert-Seifried, S.; Caironi, M.; Nielsen, M. M.; Heeney, M.; Zhang, W. M.; McCulloch, I.; Sirringhaus, H. *Adv. Mater.* **2010**, *22*, 2371–2375.
11 Xu, J. K.; Hou, J.; Zhang, S. S.; Nie, G. M.; Pu, S. Z.; Shen, L.; Xiao, Q. *J. Electroanal. Chem.* **2005**, *578*, 345–355.
12 Dong, B.; Xing, Y. H.; Xu, J. K.; Zheng, L. Q.; Hou, J.; Zhao, F. *Electrochim. Acta* **2008**, *53*, 5745–5751.
13 Zade, S. S.; Bendikov, M. *Org. Lett.* **2006**, *8*, 5243–5246.
14 Zade, S. S.; Bendikov, M. *Chem. Eur. J.* **2008**, *14*, 6734–6741.
15 Zade, S. S.; Zamoshchik, N.; Bendikov, M. *Chem. Eur. J.* **2009**, *15*, 8613–8624.
16 Bhattacharyya, D.; Gleason, K. K. *J. Mater. Chem.* **2012**, *22*, 405–410.
17 Özkut, M.; Atak, S.; Önal, A. M.; Cihaner, A. *J. Mater. Chem.* **2011**, *21*, 5268–5272.
18 Clarke, T. M.; Ballantyne, A. M.; Tierney, S.; Heeney, M.; Duffy, W.; McCulloch, I.; Nelson, J.; Durrant, J. R. *J. Phys. Chem. C* **2010**, *114*, 8068–8075.
19 Dataa, P.; Lapkowskia, M.; Motyka, R.; Suwinskia, J. *Electrochim. Acta* **2012**, *59*, 567–572.
20 Cetin, G. A.; Balan, A.; Durmus, A.; Günbas, G.; Toppare, L. *Org. Electron.* **2009**, *10*, 34–41.
21 Chung, D. S.; Kong, H.; Yun, W. M.; Cha, H.; Shim, H. K.; Kim, Y. H.; Park, C. E. *Org. Electron.* **2010**, *11*, 899–904.
22 Jo, Y. R.; Lee, S. H.; Lee, Y. S.; Hwang, Y. H.; Pyo, M.; Zong, K. *Synth. Met.* **2011**, *161*, 1444–1447.
23 Arslan Udum, Y.; Tarkuc, S.; Toppare, L. *Synth. Met.* **2009**, *159*, 361–365.
24 Gupta, A.; Choudhary, N.; Agarwal, P.; Tandon, P.; Gupta; V. D. *Synth. Met.* **2012**, *162*, 314–325.
25 Lu, B. Y.; Chen, S.; Xu, J. K.; Zhao, G. Q. *Synth. Met.* **2013**, *183*, 8–15.
26 Elschner, A.; Kirchmeyer, S.; Lvenich, W.; Merker, U.; Reuter, K. *PEDOT: Principles and application of an intrinsically conductive polymer*, Taylor & Francis Group: Boca Raton, **2011**.
27 Beaujuge, P. M.; Reynolds, J. R. *Chem. Rev.* **2010**, *110*, 268–320.
28 Chochos, C. L.; Choulis, S. A. *Prog. Polym. Sci.* **2011**, *36*, 1326–1414.
29 Yang, R. Q.; Tian, R. Y.; Yan, J. G.; Zhang, Y.; Yang, J.; Hou, Q.; Yang, W.; Zhang, C.; Cao, Y. *Macromolecules* **2005**, *38*, 244–253.
30 Aydemir, K.; Tarkuc, S.; Durmus, A.; Gunbas, G. E.; Toppare, L. *Polymer* **2008**, *49*, 2029–2032.
31 Zhu, S. S.; Swager, T. M. *J. Am. Chem. Soc.* **1997**, *119*, 12568–12577.
32 Gaupp, C. L.; Welsh, D. M.; Rauh, R. D.; Reynolds, J. R. *Chem. Mater.* **2002**, *14*, 3964–3970.
33 Reeves, B. D.; Grenier, C. R. G.; Argun, A. A.; Cirpan, A.; McCarley, T. D.; Reynolds, J. R. *Macromolecules* **2004**, *37*, 7559–7569.
34 Frisch, M. J.; Trucks, G. W.; Schlegel, H. B.; Scuseria, G. E.; Robb, M. A.; Cheeseman, J. R.; Montgomery, J. A.; Jr., Vreven, T.; Kudin, K. N.; Burant, J. C.; Millam, J. M.; Iyengar, S. S.; Tomasi, J.; Barone, V.; Mennucci, B.; Cossi, M.; Scalmani, G.; Rega, N.; Petersson, G. A.; Nakatsuji, H.; Hada, M.; Ehara, M.; Toyota, K.; Fukuda, R.; Hasegawa, J.; Ishida, M.; Nakajima, T.; Honda, Y.; Kitao, O.; Nakai, H.; Klene, M.; Li, X.; Knox, J. E.; Hratchian, H. P.; Cross, J. B.; Adamo, C.; Jaramillo, J.; Gomperts, R.; Stratmann, R. E.; Yazyev, O.; Austin, A. J.; Cammi, R.; Pomelli, C.; Ochterski, J. W.; Ayala, P. Y.; Morokuma, K.; Voth, G. A.; Salvador, P.; Dannenberg, J. J.; Zakrzewski, V. G.; Dapprich, S.; Daniels, A. D.; Strain, M. C.; Farkas, O.; Malick, D. K.; Rabuck, A. D.; Raghavachari, K.; Foresman, J. B.; Ortiz, J. V.; Cui, Q.; Baboul, A. G.; Clifford, S.; Cioslowski, J.; Stefanov, B. B.; Liu, G.; Liashenko, A.; Piskorz, P.; Komaromi, I.; Martin, R. L.; Fox, D. J.; Keith, T.; Al-Laham, M. A.; Peng, C. Y.; Nanayakkara, A.; Challacombe, M.; Gill, P. M. W.; Johnson, B.; Chen, W.; Wong, M. W.; Gonzalez, C.; Pople, J. A.; Gaussian 03, Revision C.02; Gaussian, Inc.: Wallingford CT, **2004**.
35 Parr, R. G.; Yang, W. *Density-functional Theory of Atoms and Molecules*, Oxford University Press, New York, **1989**.
36 Koch, W.; Holthausen, M. C. *A Chemist's Guide to Density Functional Theory*, Wiley-VCH, New York, **2000**.
37 Lee, C.; Yang, W.; Parr, R. G. *Phys. Rev. B* **1988**, *37*, 785–789.
38 Becke, A. D. *J. Chem. Phys.* **1993**, *98*, 5648–5652.
39 Lu, B. Y.; Yan, J.; Xu, J. K.; Zhou, S. Y.; Hu, X. J. *Macromolecules* **2010**, *43*, 4599–4608.

40 Lu, B. Y.; Xu, J. K.; Li, Y. Z.; Liu, C. C.; Yue, R. R.; Sun, X. X. *Electrochim. Acta* **2010**, *55*, 2391–2397.

41 Innis, P. C.; Mazurkiewicz, J.; Nguyen, T.; Wallace, G. G.; Macfarlane, D. *Curr. Appl. Phys.* **2004**, *4*, 389–393.

42 Li, M. C.; Ma, C. A.; Liu, B. Y.; Jin, Z. M. *Electrochem. Commun.* **2005**, *7*, 209–212.

43 Lakowicz, J. R. *Principles of Fluorescence Spectroscopy*, 2nd ed., Kluwer Academic/Plenum, New York, *1999*.

44 Lu, B. Y.; Xu, J. K.; Fan, C. L.; Miao, H. M.; Shen, L. *J. Phys. Chem. B* **2009**, *113*, 37-48.

45 Zhang, S. M.; Qin, L. Q.; Lu, B. Y.; Xu, J. K. *Electrochim. Acta* **2013**, *90*, 452–460.

46 Inzelt, G.; Pineri, M.; Schultze, J. W.; Vorotyntsev, M. A. *Electrochim. Acta* **2000**, *45*, 2403–2421.

47 Vorotyntsev, M. A.; Badiali, J. P. *Electrochim. Acta* **1994**, 39, 289–306.

48 Uckert, F.; Tak, Y. H.; Müllen, K.; Bässler, H. *Adv. Mater.* **2000**, *12*, 905–908.

Graphical Abstract:

Highly Stable Hybrid Selenophene-3,4-Ethylenedioxythiophene as Electrically Conducting and Electrochromic Polymers

Baoyang Lu, Shijie Zhen, Shimin Zhang, Jingkun Xu*, Guoqun Zhao*